Journal of The Electrochemical Society, **152** (12) A2273-A2280 (2005)
0013-4651/2005/152(12)/A2273/8/$7.00 © The Electrochemical Society, Inc.

Electrochemical Properties of $LiMn_{1-x}M_xO_2$ (M = Ni, Al, Mg) as Cathode Materials in Lithium-Ion Cells

P. Suresh,[a] A. K. Shukla,[a] and N. Munichandraiah[b,*,z]

[a]*Solid State and Structural Chemistry Unit, Indian Institute of Science, Bangalore 560012, India*
[b]*Department of Inorganic and Physical Chemistry, Indian Institute of Science, Bangalore 560012, India*

Layered $LiMn_{1-x}M_xO_2$ (M = Ni, Al, Mg) has been synthesized over a wide range of composition by ion-exchange from their sodium precursors and characterized. Both the lattice parameters (*a* and *c*) of the hexagonal unit cell increase with *x* for Ni and Mg substitutions but decrease for Al substitution. As reflected by the broad powder X-ray diffraction peaks, scanning electron micrographs show agglomeration of submicrometer-size particles. The discharge capacity of these cathode materials varies with the nature and concentration of the substituents. $LiMn_{0.95}Ni_{0.05}O_2$ exhibits a specific capacity of about 220 mAh g^{-1} during the initial cycling, which decays gradually to about 150 mAh g^{-1} after 30 charge-discharge cycles. $LiMn_{0.95}Al_{0.05}O_2$ and $LiMn_{0.95}Mg_{0.05}O_2$ yield capacity values of 180 and 150 mAh g^{-1}, respectively. Cyclic voltammetry, galvanostatic intermittent titration, and ac impedance data corroborate the observed discharge capacity behavior of these cathode materials.
 [DOI: 10.1149/1.2073067]

Manuscript submitted April 19, 2005; revised manuscript received July 19, 2005. Available electronically October 13, 2005.

The synthesis of layered $LiCoO_2$ and demonstration of topotactic extraction and insertion of Li in its interlayer space by Mizushima et al.[1] led to successful commercialization of Li-ion battery by Sony Energy Tech, Japan, in 1990. Even today, a majority of commercial Li-ion cells employs $LiCoO_2$ as the positive electrode material. On charging the cell, Li is extracted from $LiCoO_2$ and inserted into the layers of carbon negative electrode through the electrolyte. The reverse process occurs during the cell discharge. $LiCoO_2$ electrode can be cycled over a composition range corresponding to the extraction and insertion of 50% Li.[2] This corresponds to a discharge capacity of nearly 150 mAh g^{-1}. If the extraction of Li from $LiCoO_2$ exceeds 50%, its electrochemical activity gradually decays on repeated charge–discharge cycling due to structural changes. For to this reason, there have been intensive investigations on alternative compounds for positive electrodes in recent years[3-5] so as to replace the costly and toxic $LiCoO_2$ with cost-effective, stable, nontoxic compounds. Besides, it is desirable that the compound provides a high specific capacity without undergoing structural changes during the long cycle-life of the cell.

Layered $LiMnO_2$, which is isostructural with $LiCoO_2$, is considered as an alternative to $LiCoO_2$ due to its high capacity, low cost, and nontoxicity,[6] but layered $LiMnO_2$ synthesized from aqueous solutions exhibits undesirable stoichiometries with water or protons as impurities and undergoes rapid structural changes during cycling.[7,8] Recently, Armstrong and Bruce[9] have successfully synthesized the layered, anhydrous, and stoichiometric $LiMnO_2$ by ion exchange from $NaMnO_2$ in nonaqueous media. In brief, the parent sodium compound has been synthesized by solid-state reaction between stoichiometric quantities of Na_2CO_3 and Mn_2O_3. $LiMnO_2$ has been obtained by refluxing $NaMnO_2$ in *n*-hexanol containing an excess of LiCl or LiBr.[9] The charge–discharge cycling of this oxide has provided a capacity value of 200 mAh g^{-1}, which decays rapidly on cycling.[9]

Armstrong et al.[10] have synthesized and characterized $LiMn_{1-x}Co_xO_2$ with varying concentrations of Co. Among these, the compound with $x = 0.1$ has been shown to exhibit a capacity of 210 mAh g^{-1} in the first cycle with a gradual decay to 200 mAh g^{-1} after 20 cycles. With an increase in cobalt concentration to $x = 0.15$, there is an increase in capacity retention but with concomitant decrease in the overall capacity value. Capitaine et al.,[11] too, have synthesized layered $LiMnO_2$ by ion-exchange from $NaMnO_2$ precursor and have reported its structural and thermal properties. Partial substitution of Ni in $LiMnO_2$ up to 20% has been reported by Quine et al.[12] The electrochemical activity of the compounds has been shown to depend on the concentration of Ni as also on the nonaqueous medium used for Na^+/Li^+ exchange during synthesis. $LiMn_{1-x}Al_xO_2$ samples have been synthesized by Jang et al.[13] by an aqueous route, and their structural and electrochemical characterization has been reported. During electrochemical cycling, two voltage plateaus are found to develop, suggesting spinel-like phase formation, and a capacity value of 148 mAh g^{-1} has been obtained.

From the foregoing, it is found that the substitution in layered $LiMnO_2$ has been limited to only a few studies.[10-13] In brief, substitution of Ni in $LiMnO_2$ has been studied only up to 20% with no studies reported at higher substitutions of Ni. The substitution of Mn by Al in $LiMnO_2$ has been reported only from an aqueous route. Besides, $LiMn_{1-x}Mg_xO_2$ oxides have not been synthesized and studied for their electrochemical properties, even though Mg-substituted lithium manganese oxides are synthesized from the corresponding sodium bronzes.[14]

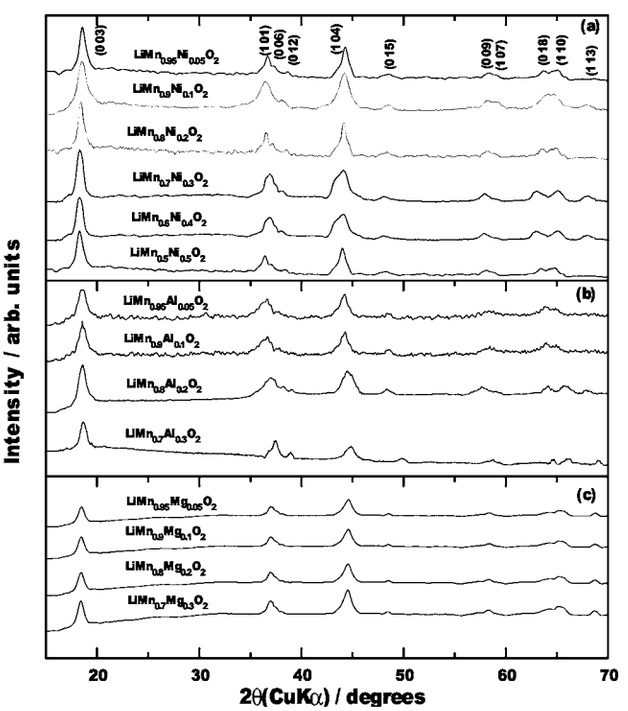

Figure 1. Powder XRD patterns for the (a) Ni-, (b) Al-, and (c) Mg-substituted $LiMnO_2$.

* Electrochemical Society Active Member.
z E-mail: muni@ipc.iisc.ernet.in

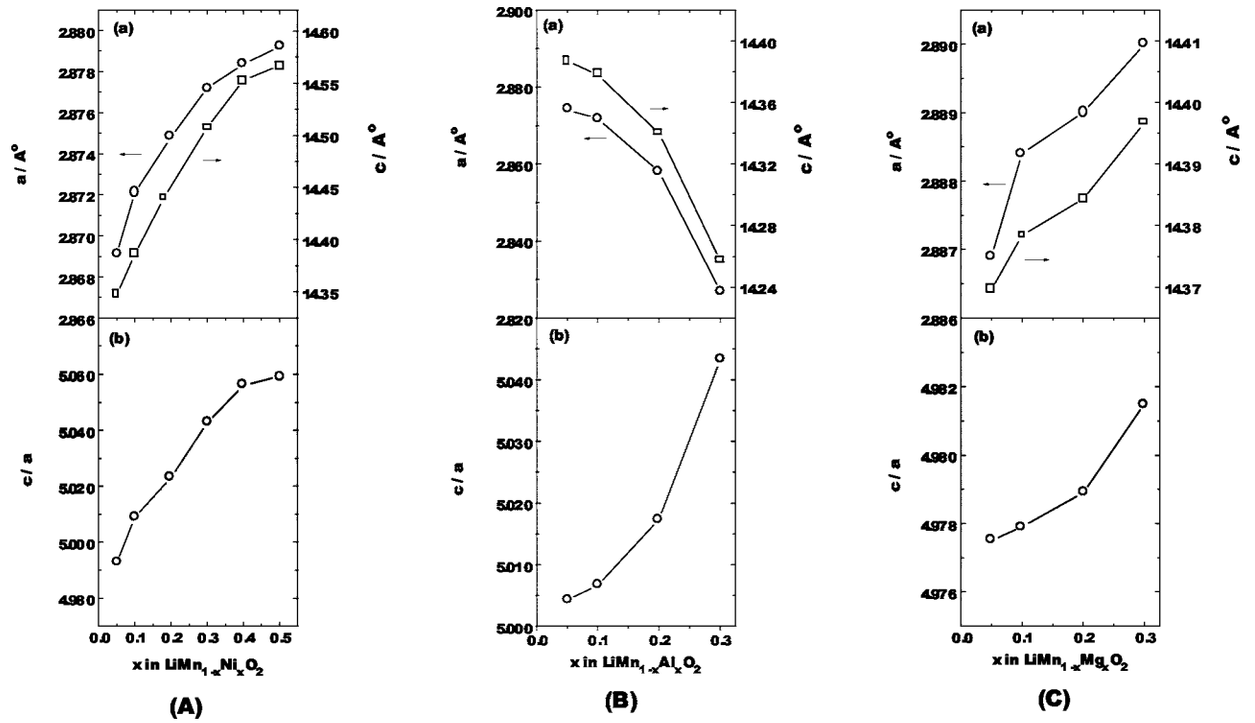

Figure 2. Variation in lattice parameters *a*, *c*, and *c*/*a* for (A) Ni-, (B) Al-, and (C) Mg-substituted $LiMnO_2$.

In the present study, $LiMn_{1-x}M_xO_2$ (M = Ni, Al, Mg) were synthesized over a wide composition range, namely, $0 \leqslant x \leqslant 0.5$ for Ni, and $0 \leqslant x \leqslant 0.3$ for Al and Mg. The compounds were subjected to a range of electrochemical studies in addition to their physicochemical characterization. The results of powder x-ray diffraction (XRD), Fourier transform infrared spectroscopy (FTIR), scanning electron microscopy (SEM), inductively coupled plasma analysis (ICP), and energy-dispersive analysis of X-rays (EDAX) studies were analyzed in conjunction with cyclic voltammetry, galvanostatic charge–discharge cycling, cycle-life, ac impedance, and galvanostatic intermittent titration data.

Experimental

$NaMn_{1-x}M_xO_2$ (M = Ni, Al, Mg; $0 \leqslant x \leqslant 0.5$ for Ni; $0 \leqslant x \leqslant 0.3$ for Al and Mg) were synthesized by preparing mixed solutions comprising stoichiometric amounts of Na_2CO_3 (Sarabhai Chemicals), $Mn(CH_3CO_2)_2{\cdot}4H_2O$ (Spectrochem), $Ni(CH_3CO_2)_2{\cdot}4H_2O$ (Loba Chemie), or $Al(NO_3)_3{\cdot}H_2O$ (S.D. Fine Chemicals) or $Mg(NO_3)_2{\cdot}6H_2O$ (Ranbaxy) in doubly distilled water. Following rotary evaporation at 80°C, the solid residue was subjected to mechanical grinding for about 30 min and heated in air at 250°C for 12 h followed by heating at 700°C for 1 h before quenching to room temperature. The product $NaMn_{1-x}M_xO_2$ (about 2 g each) was then subjected to Na^+/Li^+ ion exchange by refluxing at 140–160°C for 8 h in 30 mL of *n*-hexanol consisting of 8 M LiBr to obtain the corresponding $LiMn_{1-x}M_xO_2$. The product was cooled, filtered, washed copiously with a mixture of ethanol and methanol, and dried at 80°C for about 12 h.

Chemical analyses of the samples were carried out for Na and Li using ICP Varian Vista-pro CCB. The analyses for Mn, Ni, Al, and Mg were carried out by EDAX (JEOL JSM 5600LV). The compounds were characterized by powder XRD with Cu Kα as the source (Siemens D5005), SEM (JEOL JSM 5600LV), and FTIR spectroscopy in KBr pellets (Perkin Elmer Spectrum 1000).

For electrochemical characterization, electrodes were prepared by mixing the oxide sample, acetylene black, and polyvinylidene fluoride (Aldrich) in a weight ratio of 85:10:5. *N*-methyl pyrrolidinone (Aldrich) was used to obtain a paste of the mixture, which was coated on an Al foil (0.2 μm thick and 0.75 cm^2 area) provided with a tag for electrical connection. The Al foil was previously polished with emery, washed with double-distilled water, rinsed with acetone, and dried in a vacuum desiccator. The loading of active material was 6 mg cm^{-2}. Cells were assembled in an argon-filled glove box (MBraun, UNILAB) using Li as both counter and reference electrodes. The values of electrode potentials are given against Li/Li^+ reference electrode. The electrolyte was 1 M $LiBF_4$ in a mixture of ethylene carbonate and dimethyl carbonate (1:1 by volume). Celgard (2400) porous polypropylene film was used as the interelectrode separator.

Cyclic voltammograms (CVs) were recorded using an EG&G PARC potentiostat–galvanostat (model Versastat). Impedance spectra were recorded using an EG&G impedance analyzer (model 6310) with an excitation signal of 5 mV in the frequency range between 100 kHz and 10 mHz. Galvanostatic charge–discharge cycling was performed at C/7 rate using a circuit comprising a regulated dc power source and a high resistance ammeter in series. Cell voltage was measured using a digital multimeter with high input impedance. Galvanostatic intermittent titration (GITT) measurements were performed using a Ecochemie potentiostat–galvanostat (model Autolab PGSTAT 30).

Table I. Ionic radii of elements with coordination number 6.[30]

	Ionic radii (Å) for various oxidation states			
Ion	+1	+2	+3	+4
Li	0.76			
Mg		0.72		
Mn		0.83	0.58	0.53
Ni		0.69	0.56	
Al			0.54	

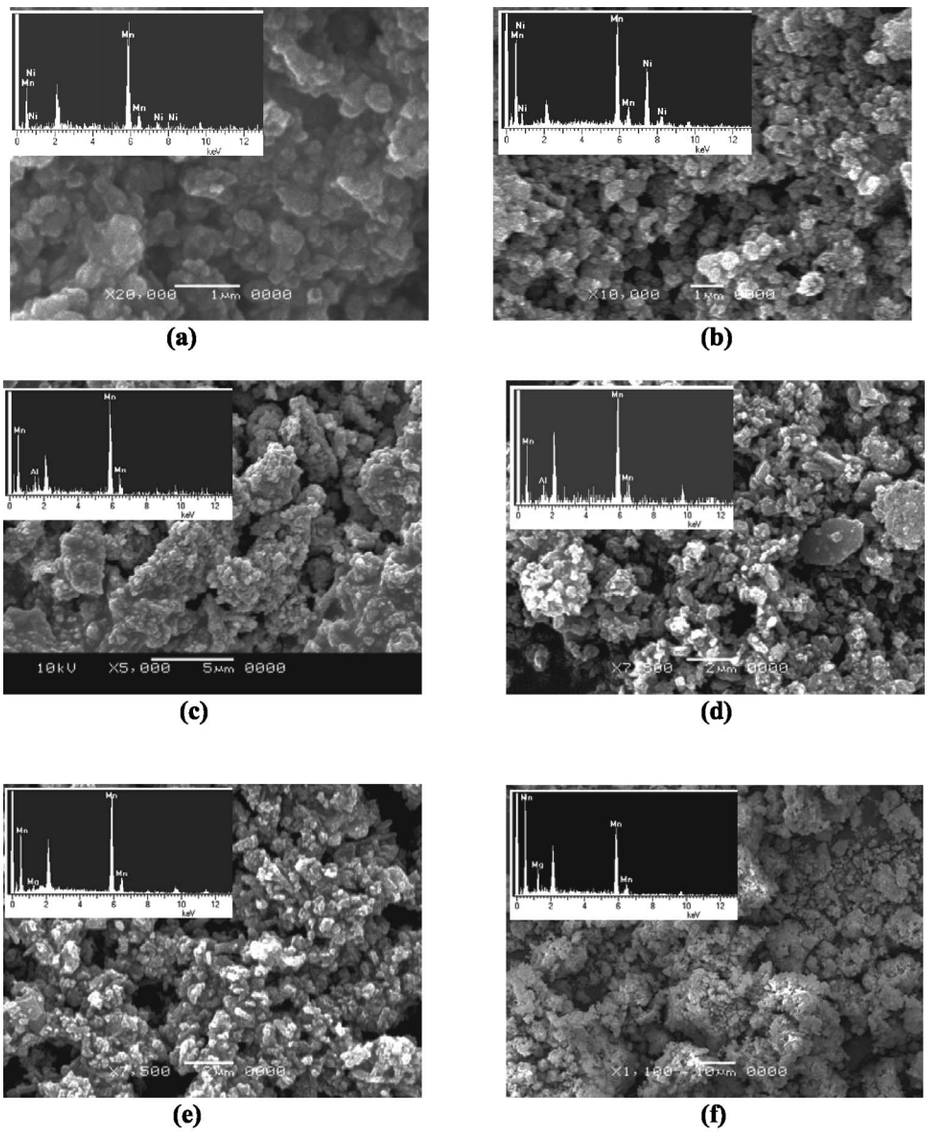

Figure 3. SEM images for (a) $LiMn_{0.9}Ni_{0.1}O_2$, (b) $LiMn_{0.7}Ni_{0.3}O_2$, (c) $LiMn_{0.9}Al_{0.1}O_2$, (d) $LiMn_{0.7}Al_{0.3}O_2$, (e) $LiMn_{0.9}Mg_{0.1}O_2$, and (f) $LiMn_{0.7}Mg_{0.3}O_2$. Corresponding EDAX patterns are shown in the insets.

Results and Discussion

XRD studies.— Powder XRD patterns of $LiMn_{1-x}M_xO_2$ (M = Ni, Al, Mg) samples are shown in Fig. 1a-c. XRD patterns for all the compositions are indexed to a hexagonal unit cell with $R\bar{3}m$ space group. The Ni-substituted samples in Fig. 1a show (006) (102) and (018) (110) pairs of peaks, suggesting well-developed layered structures for $LiMn_{1-x}Ni_xO_2$ with $x = 0.05–0.5$.[15] The variation in lattice parameters a and c with Ni concentration are shown in Fig. 2A (a), and the c/a ratio in Fig. 2A (b). It is seen that there is an increase in a, c, and c/a with an increase in x. Quine et al.[12] have reported that Ni is present as Ni^{2+} in these compounds, and the substitution of Mn^{3+} by Ni^{2+} brings about an increase in the lattice parameters. The ionic radii values, at different oxidation states for Mn and other substituents, are summarized in Table I. The increase in a and c with x as shown in Fig. 2A (a) is in accordance with larger ionic radius of Ni^{2+} in relation to Mn^{3+}.

XRD patterns of the $LiMn_{1-x}Al_xO_2$ ($x = 0–0.3$) samples are shown in Fig. 1b. It is seen that as Al concentration increases, the separation between (006) (102) and (018) (110) peaks increases, suggesting an increase in the stability of the layered structure. This is due to a decrease in concentration of Mn^{3+} that reduces the

Table II. Aimed at and observed compositions of the substituted $LiMnO_2$.

Aimed at compositions	Observed compositions
$LiMn_{0.95}Ni_{0.05}O_2$	$Na_{0.012}Li_{0.893}Mn_{0.948}Ni_{0.052}O_2$
$LiMn_{0.9}Ni_{0.1}O_2$	$Na_{0.013}Li_{0.895}Mn_{0.894}Ni_{0.106}O_2$
$LiMn_{0.8}Ni_{0.2}O_2$	$Na_{0.009}Li_{0.889}Mn_{0.797}Ni_{0.203}O_2$
$LiMn_{0.7}Ni_{0.3}O_2$	$Na_{0.009}Li_{0.892}Mn_{0.715}Ni_{0.285}O_2$
$LiMn_{0.6}Ni_{0.4}O_2$	$Na_{0.011}Li_{0.893}Mn_{0.605}Ni_{0.395}O_2$
$LiMn_{0.5}Ni_{0.5}O_2$	$Na_{0.012}Li_{0.894}Mn_{0.498}Ni_{0.502}O_2$
$LiMn_{0.95}Al_{0.05}O_2$	$Na_{0.009}Li_{0.895}Mn_{0.945}Al_{0.055}O_2$
$LiMn_{0.9}Al_{0.1}O_2$	$Na_{0.011}Li_{0.893}Mn_{0.902}Al_{0.098}O_2$
$LiMn_{0.8}Al_{0.2}O_2$	$Na_{0.012}Li_{0.895}Mn_{0.801}Al_{0.199}O_2$
$LiMn_{0.7}Al_{0.3}O_2$	$Na_{0.012}Li_{0.894}Mn_{0.711}Al_{0.289}O_2$
$LiMn_{0.95}Mg_{0.05}O_2$	$Na_{0.015}Li_{0.795}Mn_{0.961}Mg_{0.039}O_2$
$LiMn_{0.9}Mg_{0.1}O_2$	$Na_{0.011}Li_{0.800}Mn_{0.912}Mg_{0.088}O_2$
$LiMn_{0.8}Mg_{0.2}O_2$	$Na_{0.011}Li_{0.810}Mn_{0.822}Mg_{0.178}O_2$
$LiMn_{0.7}Mg_{0.3}O_2$	$Na_{0.014}Li_{0.766}Mn_{0.735}Mg_{0.265}O_2$

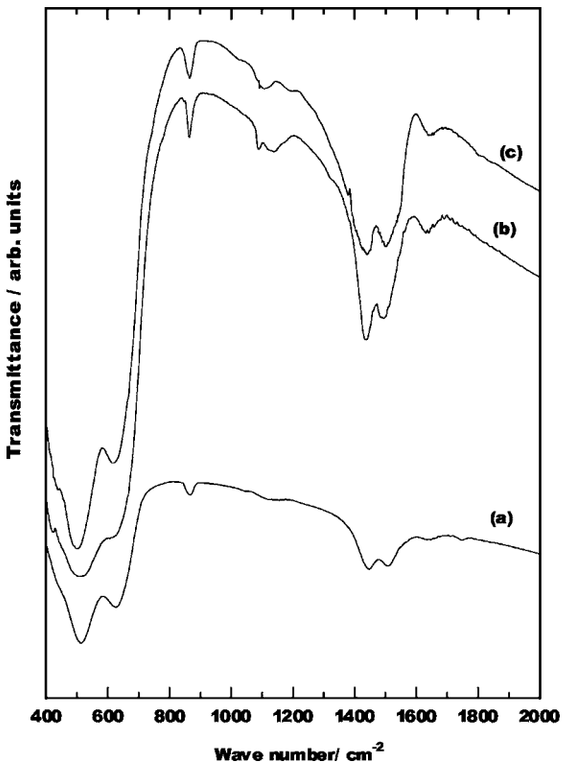

Figure 4. FTIR spectra for the (a) $LiMn_{0.9}Ni_{0.1}O_2$, (b) $LiMn_{0.9}Al_{0.1}O_2$, and (c) $LiMn_{0.9}Mg_{0.1}O_2$.

Jahn–Teller distortion. Lattice parameters were obtained for Al-substituted samples, and their variation with the Al content is shown in Fig. 2B. There is a decrease in both *a* and *c* [Fig. 2B (a)], concomitant to an increase in the *c*/*a* ratio [Fig. 2B (b)] with increase in *x*.

From the XRD patterns of $LiMn_{1-x}Mg_xO_2$ (Fig. 1c), *a*, *c*, and *c*/*a* ratio were calculated, and their variations with *x* are shown in Fig. 2C. It is seen that *a*, *c* [Fig. 2C (a)], and also *c*/*a* ratio [Fig. 2C (b)] increase with *x*. This is also attributed to the difference in size of Mg^{2+} and Mn^{3+} ions. It is reported[16] that Mg substitution in $LiCoO_2$ increases the electronic conductivity of the samples by 2 orders of magnitude. In $LiCoO_2$ or $LiNiO_2$,[17] Mg can occupy both Li and Co or Ni sites. Accordingly, in $LiMnO_2$ also, it is likely that Mg occupies both Li and Mn sites. Mg present on Li sites helps in retaining the structure during charge–discharge cycling,[16] as there is no shrinking of the interlayer separation because of comparable sizes of Mg^{2+} and Li^+ ions (Table I). Accordingly, doping of Mg is beneficial for stabilizing the $LiMnO_2$ structure. However, there is a decrease in the amount of Li for electrochemical extraction due to the presence of Mg in place of Li.

Powder XRD data of the samples $LiMn_{1-x}M_xO_2$ discussed above suggest that the layered structures are obtained with Ni, Al, and Mg as substituents up to $x = 0.5$ for Ni and $x = 0.3$ for Al and Mg. Syntheses and characterization of the compounds in the present study were restricted to these compositions as there was a decrease in electrochemical capacity with increase in *x*.

Chemical composition.— Compositional analyses of all the samples were carried out by ICP and EDAX. SEM micrographs of representative $LiMn_{0.9}M_{0.1}O_2$ and $LiMn_{0.7}M_{0.3}O_2$ samples for all the three substituents are shown in Fig. 3, with corresponding EDAX patterns as insets. SEM images show agglomeration of submicrometer-size particles, which is also reflected by the broad XRD peaks (Fig. 1). XRD patterns of the sodium phases (not shown), however, depicted intense XRD peaks and the SEM images (not shown) showed large particles. Similar observations were made

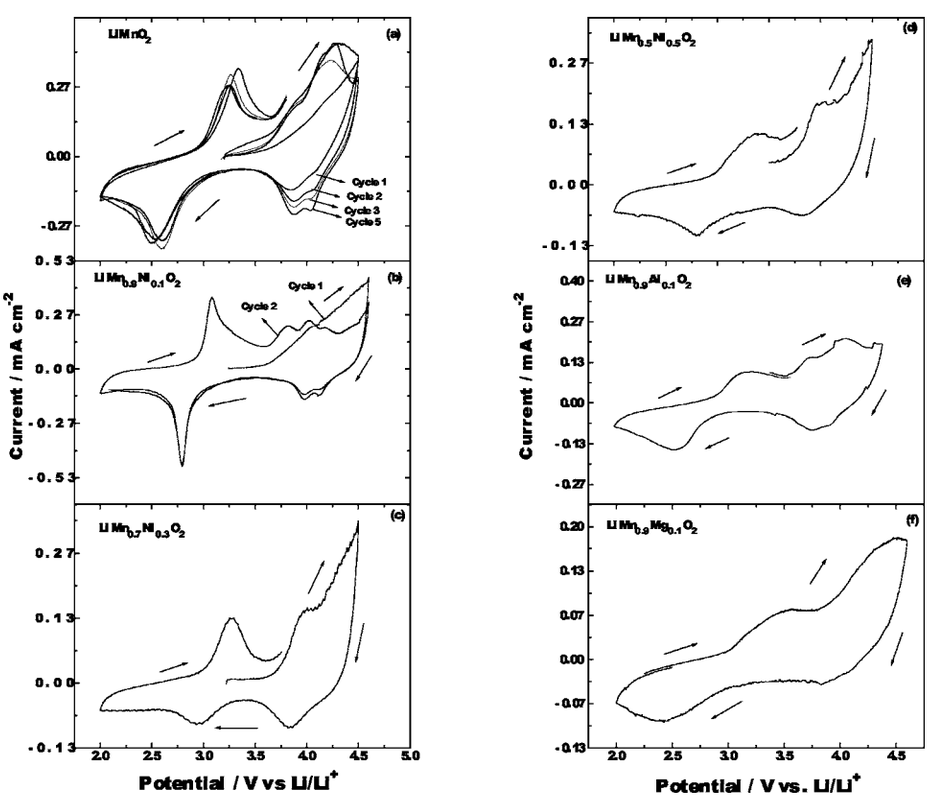

Figure 5. CVs for the (a) $LiMnO_2$, (b) $LiMn_{0.9}Ni_{0.1}O_2$, (c) $LiMn_{0.7}Ni_{0.3}O_2$, (d) $LiMn_{0.5}Ni_{0.1}O_2$, (e) $LiMn_{0.9}Al_{0.1}O_2$, and (f) $LiMn_{0.9}Mg_{0.1}O_2$. (Scan rate = 50 $\mu V\ s^{-1}$, active material weight 5 mg.)

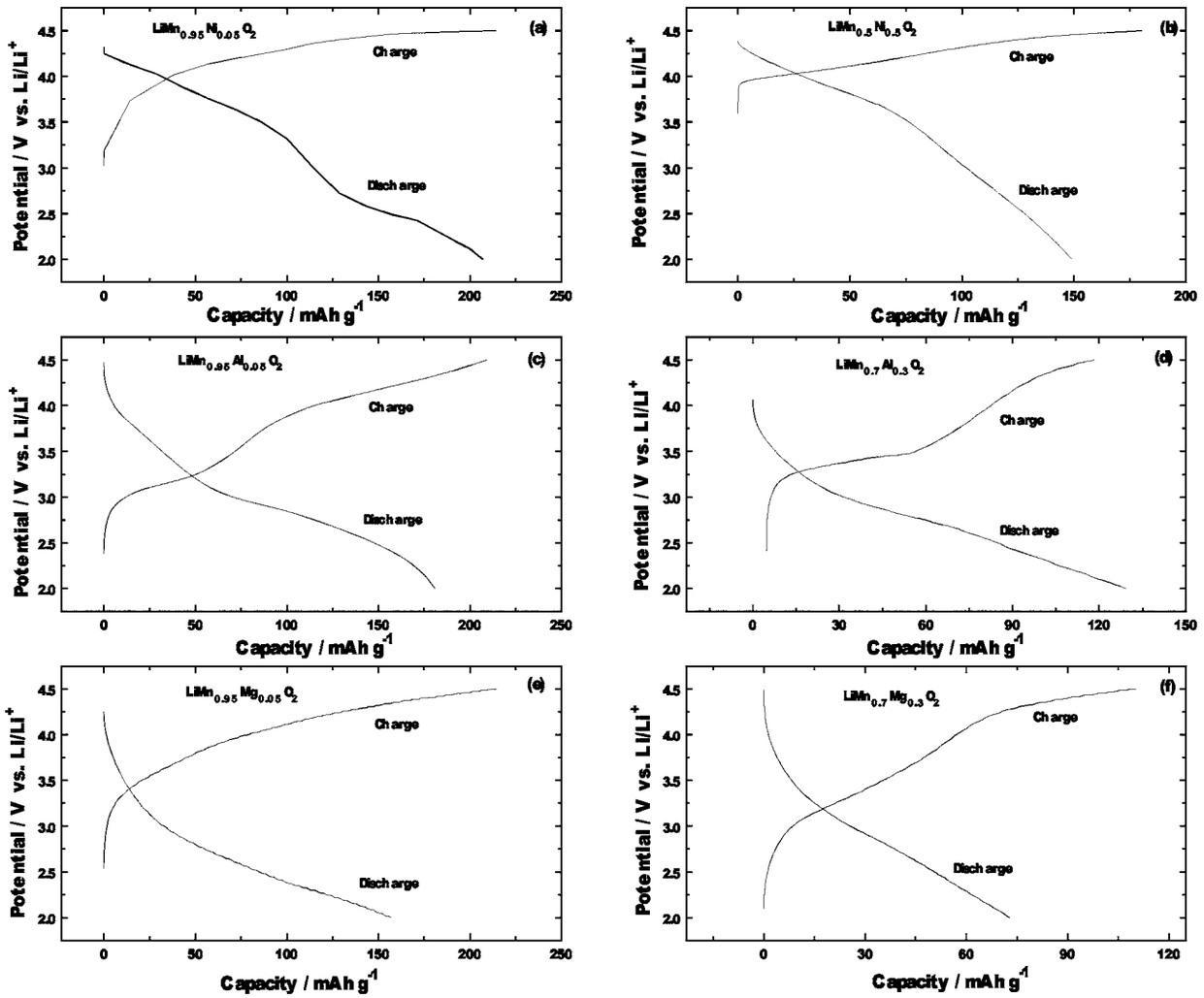

Figure 6. Charge and discharge (C/7 rate) profiles for the cells with (a) $LiMn_{0.9}Ni_{0.1}O_2$, (b) $LiMn_{0.5}Ni_{0.5}O_2$, (c) $LiMn_{0.95}Al_{0.05}O_2$, (d) $LiMn_{0.7}Al_{0.3}O_2$, (e) $LiMn_{0.95}Mg_{0.05}O_2$, and (f) $LiMn_{0.7}Mg_{0.3}O_2$ cathodes. Charge–discharge current 200 μA cm^{-2}.

with all compositions. Hence, it is inferred that there is a decrease in particle size during the Na^+/Li^+ ion-exchange process.[18] The expected and observed compositions of all the samples are listed in Table II. The total alkali metal concentration is less by about 10% than the expected composition, similar to the reported studies.[12] Furthermore, the concentration of Na is negligibly small, indicating the Na^+/Li^+ ion exchange to be close to completion.

FTIR studies.— Figure 4 shows FTIR spectra of Ni-, Al-, and Mg-substituted samples with $x = 0.1$. It is seen that the spectra of all samples are alike and there are three bands at 430, 500, and 620 cm^{-1} in the region 400–800 cm^{-1}. These bands are assigned to M–O bonds. As predicted by the group theory,[19] four bands should be observed in the region 200–900 cm^{-1} for the layered compounds with $R\bar{3}m$ space group. Another band is expected at 270 cm^{-1}, but this region could not be studied in the present experiments due to the limitation of the spectrometer. At wavenumbers higher than 800 cm^{-1}, there are three bands similar to the studies reported for the Ni-substituted $LiCoO_2$ with a layered structure.[20]

Cyclic voltammetry.— CVs were recorded for the parent compound $LiMnO_2$ and also for some of the substituted samples (Fig. 5). The CV for $LiMnO_2$ (Fig. 5a, cycle 1) shows two anodic peaks at 3.25 and 4.18 V and the corresponding cathodic peaks at 2.53 and 3.85 V. On repeated cycling, each of the peaks at 4.18 and 3.85 V split in two. This splitting of peaks suggests a gradual transformation of layered $LiMnO_2$ into a spinel phase.[21] The CV for $LiMn_{1-x}Ni_xO_2$ with $x = 0.1$, 0.3, and 0.5 are shown in Fig. 5b-d, respectively. For $x = 0.1$ composition, the voltammogram (Fig. 5b) shows a sharp anodic peak at 3.05 V, two weak peaks at 4 and 4.3 V, and the corresponding cathodic peaks at 2.8, 3.99, and 4.12 V. The pair of peaks at 3.05–2.8 V is assigned to a Mn^{3+}/Mn^{4+} reversible couple,[22] and peaks at higher potentials to Ni^{2+}/Ni^{3+} and Ni^{3+}/Ni^{4+} couples,[23] respectively. With an increase in Ni concentration, there is a decrease in ratio of Mn^{3+}/Mn^{4+} peak currents to Ni peak currents as seen from Fig. 5b-d. This is due to a decrease in the amount of electrochemically active Mn^{3+} in the compound. It is reported[24] that the 3.05 V peak for $LiMn_{0.5}Ni_{0.5}O_2$ completely disappears due to complete conversion of Mn^{3+} to Mn^{4+}. This is based on the assumption that Ni is present only as Ni^{2+}, but the presence of this peak at low intensity in the CV (Fig. 5d) suggests the presence of electrochemically active Mn^{3+} with Ni^{3+} in addition to Ni^{2+}.

CVs for the representative Al- and Mg-substituted samples are shown in Fig. 5e and f, respectively. The intensities of the peaks qualitatively indicate that the electrochemical activity of the Al-substituted samples is higher than the Mg-substituted samples. A comparison of the voltammograms of Ni-, Al-, and Mg-substituted

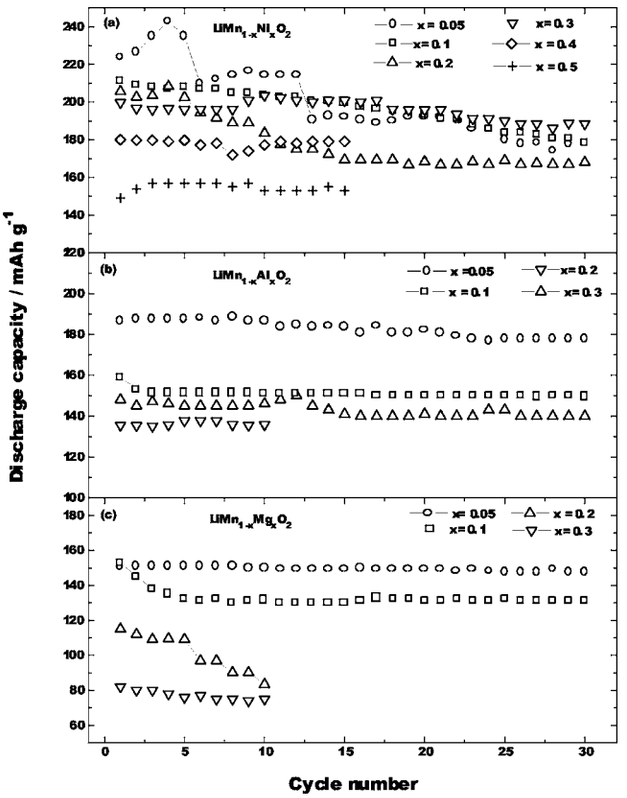

Figure 7. Cycle-life data at C/7 rate for the (a) Ni-, (b) Al-, and (c) Mg-substituted $LiMnO_2$ cathodes.

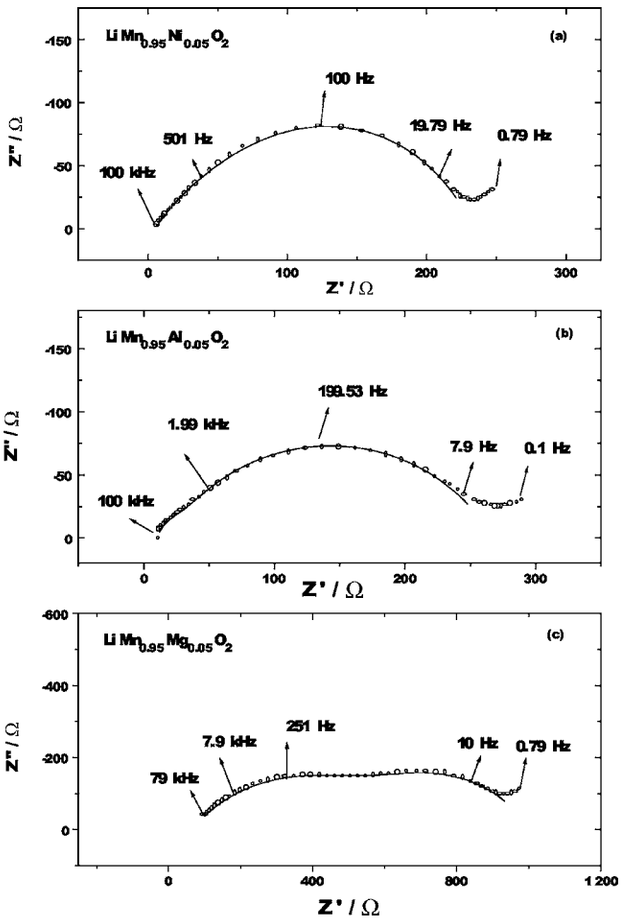

Figure 8. Nyquist plots of the impedance spectra for the (a) $LiMn_{0.95}Ni_{0.05}O_2$, (b) $LiMn_{0.95}Al_{0.05}O_2$, and (c) $LiMn_{0.95}Mg_{0.05}O_2$. The experimental data are shown with symbols and the fitted data as solid lines (active material weight 5 mg, electrode area 0.75 cm^2).

samples with $x = 0.1$ reveals that by changing the substituents from Ni through Al to Mg, the current peaks become broader. The intensity of the peaks also decreases for the electrodes of similar mass of the active material. These features suggest that the electrochemical activity decreases from Ni-, Al-, to Mg-substituted samples. This observation is also reflected in charge–discharge capacity values for the oxide materials, as described below.

Charge-discharge cycling.— Galvanostatic charge–discharge cycling of all samples was carried out in the potential region between 2 and 4.5 V. Typical potential profiles during cycling of various oxide samples are shown in Fig. 6a-f. During charging of $LiMn_{1-x}Ni_xO_2$ cathode (Fig. 6a and b), there is a rapid increase in potential initially followed by a gradual increase to 4.5 V. During discharge, there is a continuous decrease of potential from about 4.2 to 2 V. The potential profile of Al-substituted oxides (Fig. 6c and d) shows a step at about 3.5 V during charging, but there is a continuous decrease in potential during discharge. The charge–discharge curves of Mg-substituted oxide (Fig. 6e and f) are nearly similar to the data for Al-substituted samples.

Discharge capacity data for $LiMn_{1-x}M_xO_2$(M = Ni, Al, Mg) with varying compositions are shown in Fig. 7 vs the cycle numbers. Among the Ni-substituted compounds (Fig. 7a), $LiMn_{0.95}Ni_{0.05}O_2$ provides the highest capacity at 220 mAh g^{-1}, whereas the $LiMn_{0.5}Ni_{0.5}O_2$ exhibits only 150 mAh g^{-1} during the initial cycling. There is a rapid decay in capacity on repeated cycling at lower Ni contents, while a stable capacity is obtained at higher Ni contents due to a decrease in Jahn–Teller active Mn^{3+} content. Al- and Mg-substituted cathodes exhibit stable capacity values (Fig. 7b and c) for all compositions. $LiMn_{0.95}Al_{0.05}O_2$ and $LiMn_{0.95}Mg_{0.05}O_2$ cathode materials provide capacity values of 180 and 150 mAh g^{-1}, respectively. An increase in Al or Mg content results in a decrease in capacity. Thus, among Ni-, Al-, and Mg-substituted compounds, the Ni-substituted compound with $x = 0.05$ composition gives the maximum capacity but shows the higher capacity decay. Al- and Mg-substituted compounds give lower but stable capacity values. In all cases, the compound with $x = 0.05$ composition provides the highest capacity among a series of compounds.

AC impedance spectroscopy.— AC impedance technique has been used extensively for evaluation of batteries[25] and electrode materials for battery applications.[26] In the present study, after a few initial charge–discharge cycles of the electrodes, impedance spectra were recorded as shown in Fig. 8a-c. Each spectrum in the Nyquist form comprises a high-frequency intercept on the real axis, two overlapping semicircles and a low-frequency linear spike. Two semicircles have also been reported for positive electrodes of Li-ion cells in the literature.[27] The high-frequency intercept provides ohmic resistance (R_s) comprising the electrolyte resistance and the resistances of electrode material, current collectors, electrical leads, etc. While the diameter of the high-frequency semicircle gives surface film resistance (R_f), the diameter of the low-frequency semicircle provides charge-transfer resistance (R_{ct}) associated with the electrochemical process.

The impedance spectra of all compounds at several state-of-charge (SOC) values were fitted to the equivalent circuit with circuit code R(RQ)(RQ), where Q is a constant phase element, using a nonlinear least squares (NLLS) fitting program. The charge-transfer resistance (R_{ct}) at fully charged state (SOC = 1) is plotted against the composition along with their average discharge capacities in Fig.

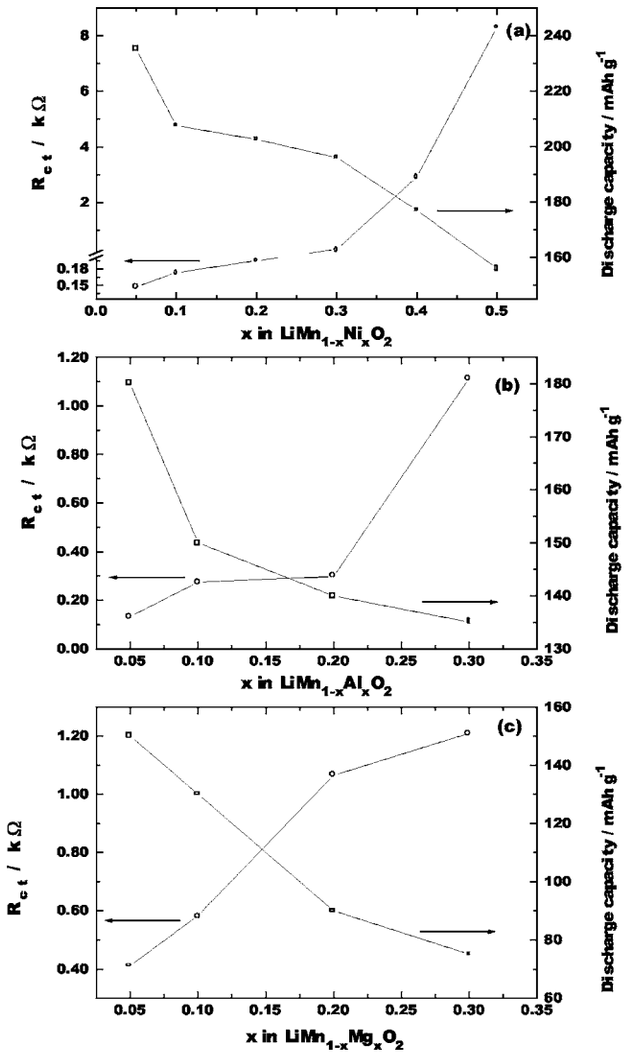

Figure 9. Variation of the charge–transfer resistance (R_{ct}, fully charged electrodes) and average discharge capacity with composition (x) for the (a) Ni-, (b) Al-, and (c) Mg-substituted $LiMn_{1-x}M_xO_2$ (active material weight 5 mg, electrode area 0.75 cm^2).

9. It is seen that there is an increase in R_{ct}, which corresponds to a decrease in capacity, with increase of substituent concentration. Accordingly, the impedance spectroscopy complements the cycling data for the compounds. A plot of R_{ct} and discharge capacity are shown for $x = 0.05$ of Ni-, Al-, and Mg-substituted compounds in Fig. 10. An increase in R_{ct}, while moving from Ni- and Al-, to Mg-substituted samples clearly reflects the capacity decrease.

Galvanostatic intermittent titration technique studies.— In the GITT technique, a $LiMn_{1-x}M_xO_2$ electrode of known composition (y) with respect to Li, i.e., y in Li_y, was subjected to lithiation or delithiation by applying a constant current (I_o) for a time τ, at the end of which the compound attained a known lithium content $y \pm \Delta y$. As a result, there was a change in its potential from its equilibrium value (E_o) that reaches E_τ at a time τ. After interruption of the current at time τ, the electrode was allowed to reach its new steady-state potential E_s, and the change in the steady-state potential $\Delta E_s (= E_s - E_o)$ was calculated. From the values of $\Delta E_\tau (= E_\tau - E_o)$ and ΔE_s, the diffusion coefficient of Li (D_{Li}) was calculated for several SOC values using Eq. 1[28]

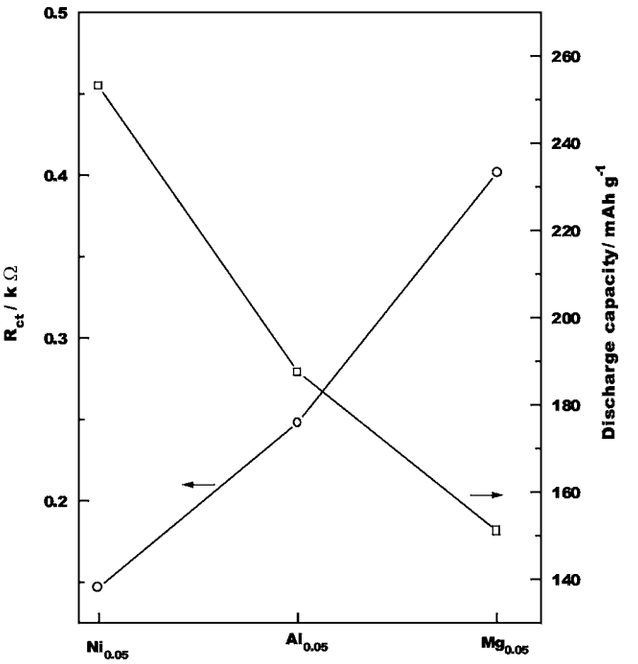

Figure 10. Variation in charge–transfer resistance and average discharge capacity for (a) $LiMn_{0.95}Ni_{0.05}O_2$, (b) $LiMn_{0.95}Al_{0.05}O_2$, and (c) $LiMn_{0.9}Mg_{0.1}O_2$ (active material weight 5 mg, electrode area 0.75 cm^2).

$$D_{Li} = (4/(\pi\tau))(m_B V_m / M_B A)^2 (\Delta E_s / \Delta E_\tau)^2 \quad [1]$$

In Eq. 1, m is the mass of the active material, M_B is molar mass, V_m is molar volume, and A is area of the electrode. Typical experimental values are $I_o = 25\ \mu A\ cm^{-2}$, $\tau = 5400$ s, $\Delta E_s = 124$ mV, $\Delta E_\tau = 252$ mV, $V_m = 20.8\ cm^3$, and $m_B = 2\ mg\ cm^{-2}$. GITT experiments were conducted for the Ni-, Al-, and Mg-substituted compounds over the potential range between 2 and 4.5 V, and D_{Li} values were calculated. The values of D_{Li} obtained were between 5×10^{-10} and 5×10^{-11} cm^2 s^{-1}, which agree well with values reported for the layered compounds $LiCoO_2$ and $LiNiO_2$.[29]

Conclusions

Layered $LiMn_{1-x}M_xO_2$ (M = Ni,Al,Mg) compounds have been synthesized by ion exchange from the corresponding sodium precursors. The discharge capacity values are found to vary with the nature and concentration of the substitution. Specific capacity obtained for $LiMn_{0.95}Ni_{0.05}O_2$ cathode is about 220 mAh g^{-1} during initial cycling but it decays to about 150 mAh g^{-1} after 30 charge–discharge cycles. With an increase in the Ni content, the initial specific capacity decreases with a lesser decay on cycling. The Al- and Mg-substituted compounds for $x = 0.05$ composition provide lower capacities of 180 and 150 mAh g^{-1}, respectively, but their capacity values remain stable on subjecting the electrodes to charge–discharge cycling. The capacity data are supported by cyclic voltammetry, GITT, and ac impedance studies.

References

1. K. Mizushima, P. C. Jones, P. J. Wiseman, and J. B. Goodenough, *Mater. Res. Bull.*, **15**, 783 (1980).
2. H. Wang, Y. I. Jang, B. Huang, D. R. Sadoway, and Y. M. Chiang, *J. Electrochem. Soc.*, **146**, 473 (1999).
3. M. S. Whittingham, *Chem. Rev. (Washington, D.C.)*, **104**, 4271 (2004).
4. T. Ohzuku, K. Ariyoshi, Y. Makimura, N. Yabuuchi, and K. Sawai, *Electrochemistry (Tokyo, Jpn.)*, **73**, 2 (2005).
5. S. Okada and J. I. Yamaki, *J. Ind. Eng. Chem. (Seoul, Repub. Korea)*, **10**, 1104 (2004).
6. B. Ammundsen and J. M. Paulsen, *Adv. Mater. (Weinheim, Ger.)*, **13**, 943 (2001).
7. M. H. Rossouw, D. C. Liles, and M. M. Thackeray, *J. Solid State Chem.*, **104**, 464 (1993).

8. M. M. Thackeray, *J. Electrochem. Soc.*, **142**, 2558 (1995).
9. A. R. Armstrong and P. G. Bruce, *Nature (London)*, **381**, 499 (1996).
10. A. R. Armstrong, R. Gitzendanner, A. D. Robertson, and P. G. Bruce, *Electrochem. Commun.* **1998**, 1833.
11. F. Capitaine, P. Gravereau, and C. Delmas, *Solid State Ionics*, **89**, 197 (1996).
12. T. E. Quine, M. J. Duncan, A. R. Armstrong, A. R. Robertson, and P. G. Bruce, *J. Mater. Chem.*, **10**, 2838 (2000).
13. Y. I. Jang, B. Huang, Y. M. Chiang, and D. R. Sadoway, *Electrochem. Solid-State Lett.*, **1**, 13 (1998).
14. M. Wei, Y. Lu, D. G. Evans, and X. Duan, *Solid State Ionics*, **161**, 133 (2003).
15. S. C. Garcia, A. C. Couceiro, M. A. S. Rodriguez, F. Soulette, and C. Julien, *Solid State Ionics*, **156**, 15 (2003).
16. H. Takamoto and A. R. West, *J. Electrochem. Soc.*, **144**, 3164 (1997).
17. C. Pouillerie, L. Croguennec, P. B. Biensan, P. Willmann, and C. Delmas, *J. Electrochem. Soc.*, **147**, 2061 (2000).
18. P. Suresh, A. K. Shukla, and N. Munichandraiah, *Electrochem. Solid-State Lett.*, **8**, A263 (2005).
19. W. Huang and R. Frech, *Solid State Ionics*, **86**, 395 (1996).
20. T. Ohzuku, A. Ueda, M. Nagayama, Y. Iwakoshi, and H. Komori, *Electrochim. Acta*, **38**, 1159 (1993).
21. G. Vitins and K. West, *J. Electrochem. Soc.*, **144**, 2587 (1997).
22. J. M. Paulsen, C. L. Thomas, and J. R. Dhan, *J. Electrochem. Soc.*, **147**, 861 (2000).
23. S. H. Kang, J. Kim, M. E. Stoll, D. Abraham, Y. K. Sun, and K. Amine, *J. Power Sources*, **112**, 41 (2002).
24. S. H. Kang and K. Amine, *J. Power Sources*, **119**, 150 (2003).
25. J. R. Macdonald, *Impedance Spectroscopy*, p. 84, John Wiley & Sons, New York (1987).
26. D. Aurbach, M. D. Levi, E. Levi, and A. Schechter, Abstract 113, p. 124, The Electrochemical Society and International Society of Electrochemistry Meeting Abstracts, Vol. 97-2, Paris, France, Aug 31-Sept. 5, 1997.
27. M. G. S. R. Thomas, P. G. Bruce, and J. B. Goodenough, *J. Electrochem. Soc.*, **132**, 1521 (1985).
28. K. M. Shaju, G. V. Subbarao, and B. V. R. Chowdari, *J. Electrochem. Soc.*, **150**, A1 (2003).
29. Y. M. Choi, S. Pyun, J. S. Bae, and S. I. Moon, *J. Power Sources*, **65**, 25 (1995).
30. *CRC Handbook of Chemistry and Physics*, 82nd ed., D. R. Lide, Editor, CRC Press, Boca Raton, FL (2001).